# Efficient Analysis and Design of Novel SIW Leaky-Wave Antenna

Alejandro Javier Martinez-Ros, *Student Member, IEEE*, José Luis Gómez-Tornero, *Member, IEEE*, and Fernando Quesada-Pereira, *Member, IEEE*

***Abstract*—A novel transverse equivalent network is developed in this letter to efficiently analyze a recently proposed leaky-wave antenna in substrate integrated waveguide (SIW) technology. For this purpose, precise modeling of the SIW posts for any distance between vias is essential to obtain accurate results. A detailed parametric study is performed resulting in leaky-mode dispersion curves as a function of the main geometrical dimensions of the antenna. Finally, design curves that directly provide the requested dimensions to synthesize the desired scanning response and leakage rate are reported and validated with experiments.**

***Index Terms*—Leaky-wave antennas (LWAs), planar antennas, substrate integrated waveguide (SIW), transverse equivalent network (TEN).**

## I. Introduction

LEAKY-WAVE antennas (LWAs) can be efficiently designed by obtaining the complex propagation constant of the radiating leaky mode ($k = \beta - j\alpha$) as a function of frequency and the main geometrical parameters of the antenna [1]. Recently, a novel planar LWA in substrate integrated waveguide (SIW) technology was proposed [see Fig. 1(a)], showing the interesting feature of simultaneous control over the leaky-mode phase and leakage rate by only modifying the SIW width $W$ and the distance between posts $P$ [2]. Previous printed-circuit LWAs, such as the microstrip [3] or the half-width microstrip [4] LWAs, did not provide this flexible control over the leaky mode, thus suffering from limitations in the tailoring of the radiation pattern. In this letter, the novelty resides in the precise modeling of the posts' equivalent T-network for any distance between vias both for the row of posts acting as perfect electric conductor (PEC) as the one acting as partially reflecting surface (PRS) [see Fig. 1(a)]. This T-network is incorporated to a transverse equivalent network (TEN) [see Fig. 1(b)], as will be illustrated in Section II. In Section III, a parametric study to provide a detailed physical insight on the influence of the main dimensions of the antenna will be shown. Particularly, the effects of the radiating strip width $W_0$ and substrate thickness $h$ are studied for the first time, showing important design constraints regarding coupling and cross-polarizations effects. Finally, Section IV shows design curves used to obtain the desired frequency scanning response, and which are validated with experimental prototypes. The proposed TEN provides a much more efficient design technique than the one used in [2], which was based on full-wave simulations of the complete 3-D computer-aided design (CAD) model of the antenna.

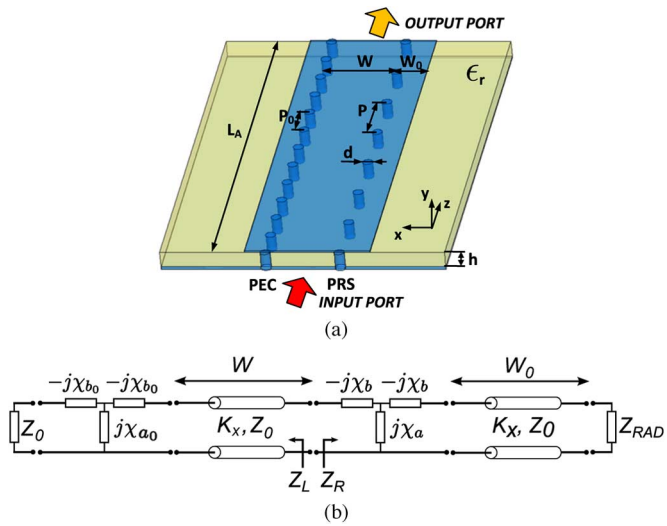


Fig. 1. (a) Scheme of novel SIW LWA. (b) Associated TEN.

## II. Efficient Leaky-Mode Analysis of a SIW LWA

The scheme of the proposed TEN is shown in Fig. 1(b). Two sections of transmission lines of lengths $W$ and $W_0$ model the SIW width and the radiating strip width, respectively. This strip is terminated on its right side by an equivalent impedance $Z_{\mathrm{RAD}}$ that characterizes the radiating discontinuity due to the truncation of the upper plate in a dielectric-filled parallel-plate waveguide [5]. Connecting the SIW and the radiating strip sections, the T-network composed by one parallel inductor and two series capacitors (with respective reactances $X_a$ and $X_b$) models the row of metallic cylinders of diameter $d$ separated at a distance $P$, as it was proposed by Marcuvitz [6, pp. 285–289]. Similar equivalent T impedance network is used at the left side of the SIW to model the row of metallic posts with period $P_0$, which is connected to the characteristic impedance $Z_0$ of the parallel-plate dielectric substrate. The analytical expressions for $X_a$ and $X_b$ proposed by Marcuvitz in [6] are limited by the small-obstacle approximation to very sparse posts ($P/d > 5$). On the contrary, the effective width models extensively used in the design of nonradiative SIW circuits are only valid for close vias ($P/d < 3$) [7] and do not allow to obtain complex leaky

Manuscript received November 09, 2012; revised February 14, 2013; accepted March 27, 2013. Date of publication April 03, 2013; date of current version April 16, 2013. This work was supported by the Ministerio de Educación y Ciencia Español the Spanish Regional Seneca Project, Ref. TEC2010-21520-C04-04, and the Spanish Regional Seneca Project 08833/PI/08.

The authors are with the Department of Communication and Information Technologies, Universidad Politécnica de Cartagena, Cartagena 30202, Spain (e-mail: alejandro.martinez@upct.es; josel.gomez@upct.es; fernando.quesada@upct.es).

Color versions of one or more of the figures in this letter are available online at http://ieeexplore.ieee.org.

Digital Object Identifier 10.1109/LAWP.2013.2256769

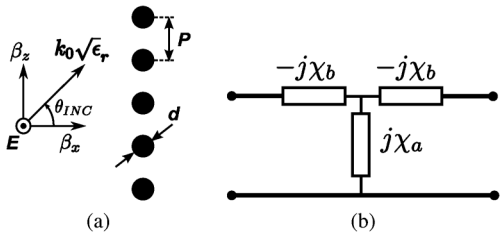


Fig. 2. (a) Scheme of TE plane-wave incidence on a row of periodic metallic posts. (b) Equivalent T-circuit model proposed by Marcuvitz [6].

modes. Therefore, there is a lack of a TEN that allows to accurately obtain the dispersion of complex leaky modes in SIW technology for any ratio $P/d$. This is of key importance for the efficient design of the novel SIW LWA whose study in [2] relied on full-wave analysis of the complete 3-D CAD model using commercial software such as HFSS.

### *A. Accurate Modeling of Partially Reflective Inductive Posts*

To overcome the restrictions of Marcuvitz's model, the reactances $X_a$ and $X_b$ are extracted from an accurate full-wave analysis of the reflection coefficient $\rho_P$ of a periodic row of metallic posts under TE plane-wave incidence, as illustrated in Fig. 2. This analysis is based on an efficient electric field integral equation (EFIE) technique, which uses the Green's function of a periodic distribution of electric current filaments accelerated with Kummers' method [8]. The reflection coefficient is then computed for the incidence angle $\theta_{\rm INC}$ [see Fig. 2(a)] and the rest of the geometrical parameters ($P$, $d$, and $\epsilon_{\rm r}$). Hence, the associated complex impedance can be then derived from $\rho_P$

$$\begin{aligned}\overline{Z_P}(P,\theta_{\rm INC}) &= \frac{Z_P}{Z_0} = \frac{1+\rho_P(P,\theta_{\rm INC})}{1-\rho_P(P,\theta_{\rm INC})} \\ &= \overline{R_P}(P,\theta_{\rm INC}) + j\overline{X_P}(P,\theta_{\rm INC}). \end{aligned} \tag{1}$$

After some algebraic manipulations, the following equations relate the normalized reactances $\overline{X_a}$ and $\overline{X_b}$ with $\overline{R_P}$ and $\overline{X_P}$, thus expressing their dependence with $P$ and $\theta_{\rm INC}$:

$$\begin{aligned}&\overline{X_a}(P,\theta_{\rm INC}) \\ &\quad = \frac{X_a}{Z_0} \\ &\quad = \sqrt{\overline{R_P}(P,\theta_{\rm INC})\left[1+\left(\frac{\overline{X_P}(P,\theta_{\rm INC})}{1-\overline{R_P}(P,\theta_{\rm INC})}\right)^2\right]}\end{aligned} \tag{2}$$

$$\begin{aligned}&\overline{X_b}(P,\theta_{\rm INC}) \\ &\quad = \frac{X_b}{Z_0} \\ &\quad = \overline{X_a}(P,\theta_{\rm INC}) - \frac{\overline{X_P}(P,\theta_{\rm INC})}{1-\overline{R_P}(P,\theta_{\rm INC})}.\end{aligned} \tag{3}$$

### *B. Development of an Accurate TEN*

Once the numerical procedure to compute $X_a$ and $X_b$ has been presented as in Section II-A, its corresponding values can be obtained for any incidence angle $\theta_{\rm INC}$ and any period $P$ and can be introduced in the TEN shown in Fig. 1(b). On the other hand, the equivalent impedances of the transmission lines sections can be readily expressed from their respective lengths $W$ and $W_0$ and using the transverse wavenumber $k_x$ and the characteristic impedance of a $TE$-polarized wave

$$Z_0(\theta_{\rm INC}) = \frac{\omega\mu_0}{k_x(\theta_{\rm INC})} \tag{4}$$

where $k_x$ can be related to the longitudinal wavenumber $k_z$ by the following expression, where $k_0$ is the free-space wavenumber and $\epsilon_{\rm r}$ the substrate permittivity [see Fig. 2(a)]:

$$k_x(\theta_{\rm INC}) = \sqrt{k_0^2\epsilon_r - k_z^2(\theta_{\rm INC})}. \tag{5}$$

Finally, the transverse resonance equation (TRE) can be expressed at the reference plane shown in Fig. 1(b) as

$$Z_L(k_z) + Z_R(k_z) = 0 \tag{6}$$

which must be solved for the unknown leaky-mode complex longitudinal wavenumber $k_z$

$$k_z(\theta_{\rm INC}) = \beta_z(\theta_{\rm INC}) - j\alpha. \tag{7}$$

It must be noticed that the internal angle of incidence $\theta_{\rm INC}$ is related to the leaky-wave phase-constant $\beta_z$ [see Fig. 2(a)] by

$$\sin\theta_{\rm INC} = \frac{\beta_z}{k_0\sqrt{\epsilon_{\rm r}}}. \tag{8}$$

Therefore, the problem of finding the leaky-mode solution is equivalent to the minimization of (6) in the complex plane $(\beta_z - j\alpha)$ [1]. As an example, Fig. 3 shows the leaky-mode normalized phase and attenuation constants ($\beta_z/k_0$ and $\alpha/k_0$) for three different values of $P$, as frequency is varied from 12 to 18 GHz. The rest of the geometrical parameters of the studied LWA are kept fixed, and they are summarized in the inset of Fig. 3(b). Results obtained from the proposed TEN are compared to HFSS and to modal results using Marcuvitz's analytical impedance. As expected, the degree of inaccuracy of Marcuvitz's results is higher for lower values of $P$ [see Fig. 3(a)] due to the aforementioned small-obstacle restrictions. On the other hand, some discrepancies between results computed by the proposed TEN and HFSS are present in Fig. 3(b) due to the assumption of uniform plane-wave incidence in the calculation of (1)–(3); which is made more significant close to the cutoff regime ($\alpha > \beta$). Nevertheless, Fig. 3 shows that the proposed TEN provides good results for all values of $P$.

## III. Parametric Dispersion Curves

In order to characterize the behavior of the proposed SIW LWA as its main geometrical parameters are varied, several dispersion curves at a fixed design frequency (15 GHz) will be obtained. In each section, it will be shown the effect of a parameter in the leaky-mode normalized leakage rate $\alpha/k_0$ and its associated radiation angle $\theta_{\rm RAD}$ given by [1]

$$\sin\theta_{\rm RAD} \approx \frac{\beta_z}{k_0}. \tag{9}$$

### *A. Effect of Distance Between Reflective Posts $P$ and SIW Width $W$*

For a fixed design frequency of 15 GHz, Fig. 4 illustrates the effect of the distance between the PRS posts' distance $P$ and different SIW widths $W$. As expected, when $P$ is increased, the PRS wall becomes more transparent, thus increasing the leakage

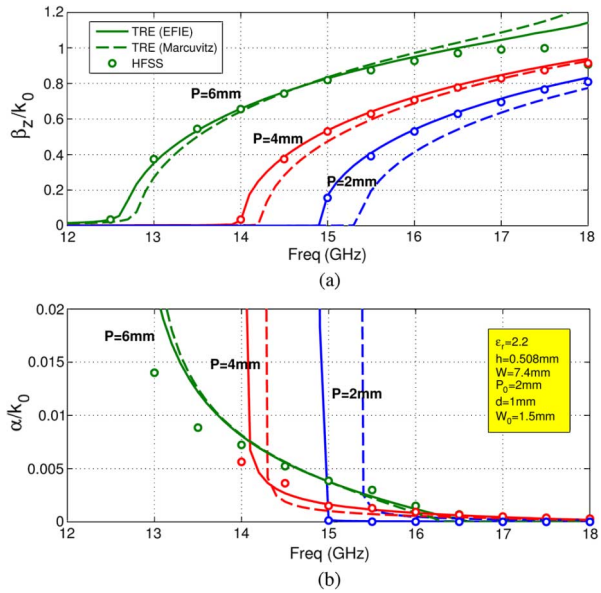


Fig. 3. (a) Normalized phase constant. (b) Normalized leakage rate as a function of frequency and different values of $P$.

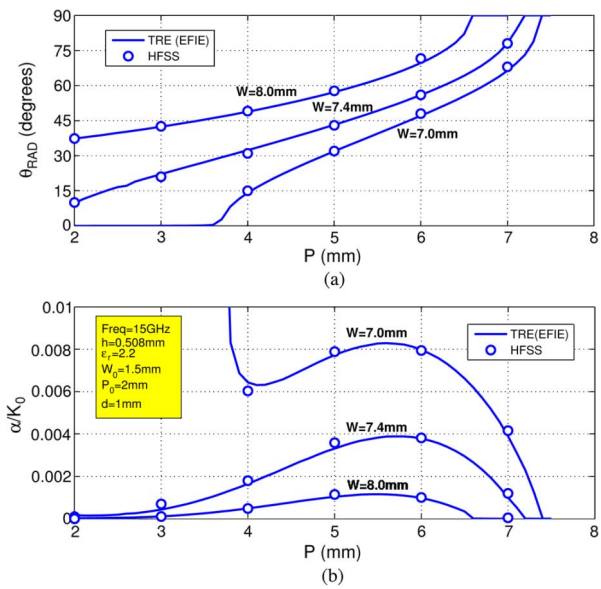


Fig. 4. (a) Pointing angle of the main beam. (b) Normalized leakage rate as a function of the separation between posts $P$ and for different widths $W$.

rate [see Fig. 4(b)]. However, it is also observed how for periods larger than ≈5.5 mm, the leakage rate starts to decrease as a result of the tendency toward endfire radiation ($\theta_{\mathrm{RAD}} \rightarrow 90°$), which ultimately vanishes the leakage when entering the surface-wave regime for $P > 7$ mm. On the other hand, $W$ modifies the cutoff frequency of the SIW leaky mode, thus provoking an increase in the scanning angle for wider strips, as shown in Fig. 4(a). In any case, good agreement is observed between HFSS and the proposed model for all studied values of $P$ and $W$.

### B. Effect of Radiating Strip Width $W_0$

The strip section of width $W_0$ acts as a transition from the fields coming through the SIW PRS wall and which reach the

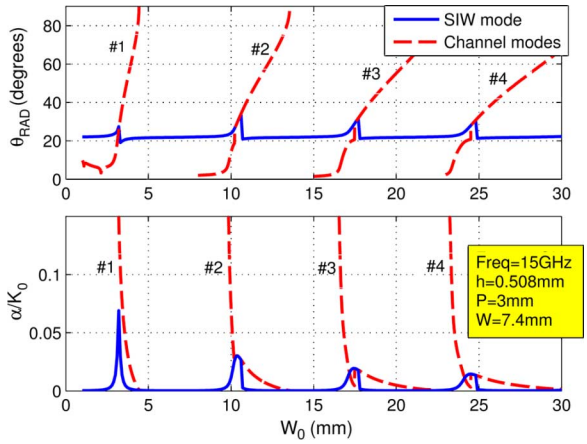


Fig. 5. Dispersion curves as a function of radiating strip width $W_0$ for SIW leaky mode and higher-order channel-guide leaky modes.

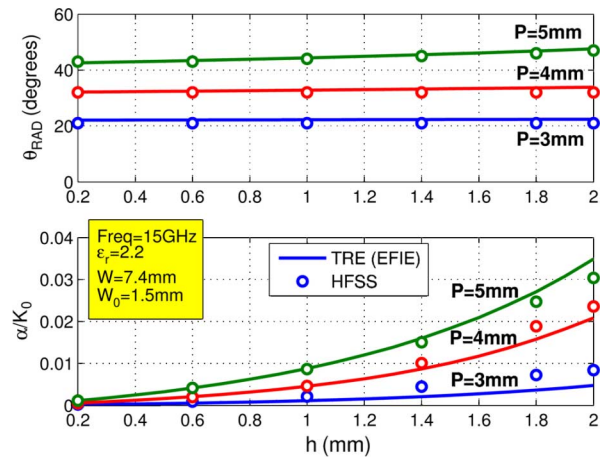


Fig. 6. Effect of the substrate thickness $h$ over the SIW leaky mode for different values of $P$.

radiating discontinuity occurring at its edge [see Fig. 1(a)]. As $W_0$ is increased, higher-order channel leaky modes [9] will start appearing. Particularly, this happens when $W_0 \approx \lambda/4$, and it is repeated every $\lambda/2$, as can be observed from the coupling between modes (when the SIW leaky mode crosses with the channel modes [9]) in Fig. 5. To avoid this undesired coupling, it is convenient to use narrow strips ($W_0 < \lambda/4$). However, there is a tradeoff since narrower strips create stronger coupling between the PRS and the radiating end [9] that results in higher cross-polarization (XP) levels due to the interaction of evanescent fields, which are not accounted for the TEN and reduce its accuracy. An optimum value of $W_0 = 1.5$ mm is chosen to minimize undesired coupling effect while assuring minimum XP discrimination (XPD) level.

### C. Effect of Substrate Thickness $h$

The dependence of the leaky mode with the substrate thickness $h$ is shown in Fig. 6. As it is observed, the pointing angle $\theta_{\mathrm{RAD}}$ remains almost constant with $h$ for each value of $P$. On the other hand, thicker substrates allow to obtain a higher range of variation in the leakage rate, as it usually happens with printed antennas [3]. Although this is something wanted, the use of thicker substrates increases the level of XP of the

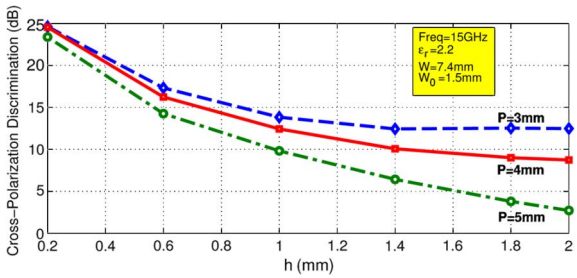


Fig. 7. Dependence of the polarization discrimination level with $h$.

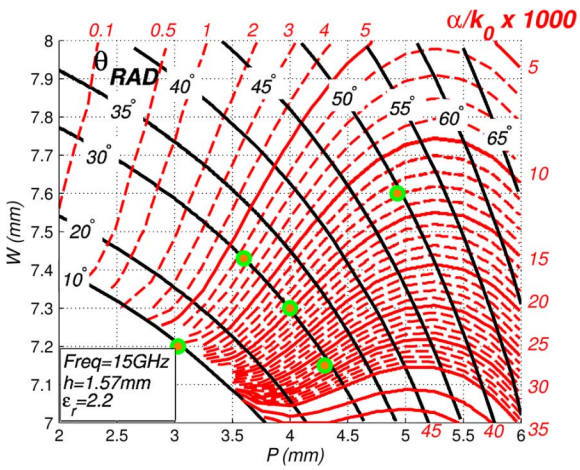


Fig. 8. Two-dimensional dispersion chart for SIW LWA, including in circles the dimensions of the five manufactured antennas in [2].

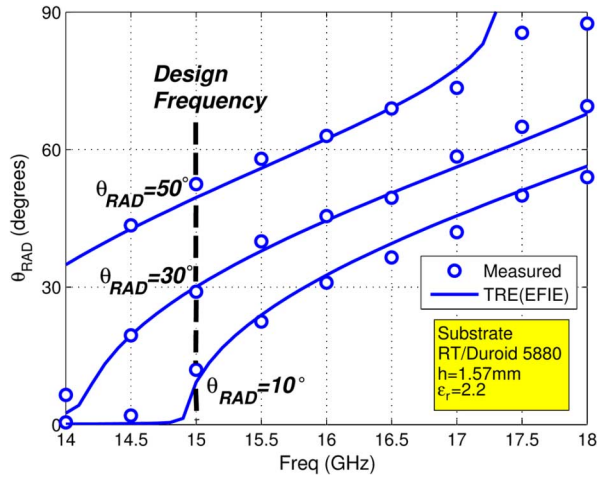


Fig. 9. Measured and simulated frequency scanning responses for the three antennas designed in [2] to radiate at $\theta_{\mathrm{RAD}} = 50°$, 30°, and 10° at the frequency of 15 GHz.

radiated fields, and thus decreases the XPD as shown in Fig. 7. Therefore, it is important to have a tradeoff between higher leakage values and higher XPD levels. Commercial substrates with standard values of $h = 0.508$ mm and $\epsilon_{\mathrm{r}} = 2.2$ offer levels of XPD over 15 dB and maximum $\alpha/k_0 = 0.005$.

## IV. Design Curves and Conclusions

As illustrated in Section III, once $W_0$ and $h$ are fixed, the two main parameters that allow to simultaneously control the leaky-mode phase and leakage rates are $W$ and $P$. Fig. 8 shows a two-dimensional dispersion chart [10], where constant-$\theta_{\mathrm{RAD}}$ and constant-$\alpha/k_0$ curves are plotted with continuous lines and dashed lines, respectively. $W$ and $P$ are simultaneously swept in all the range of useful values ($W = [7\text{ mm}, 8\text{ mm}]$, and $P = [2\text{ mm}, 6\text{ mm}]$, while the rest of the parameters are fixed to $\epsilon_{\mathrm{r}} = 2.2$, $h = 1.57$ mm, $d = 1$ mm, $P_0 = 2$ mm, and $W_0 = 1.5$ mm), and the design frequency is set to 15 GHz. As an example, it is shown with circles in Fig. 8 five points that correspond to the five LWAs designed in [2]. Each point corresponds to the set of dimensions ($W$ and $P$) that were obtained in [2] using HFSS to provide the requested values of $\theta_{\mathrm{RAD}}$ and $\alpha/k_0$. As it can be seen, three designs points lie in the constant $\theta_{\mathrm{RAD}} = 30°$ curve, but with different leakage rates, so that the scanning angle is kept constant, while the directivity (and beamwidth $\Delta\theta$) is varied as explained in [2]. The other three points lie in three different scanning curves $\theta_{\mathrm{RAD}} = 10°, 30°$, and 50°, and with the appropriate leakage rate values to provide $\Delta\theta = 10°$ beamwidth and 90% radiation efficiency [2]. The designed dimensions match the ones that were obtained in [2] with 3-D full-wave iterative optimization (trial and error) using HFSS. Clearly, the computational cost needed for the modal dispersion synthesis technique proposed in this work is much lower than the design approach of [2]. Finally, Fig. 9 illustrates the frequency scanning responses for the three LWAs designed in [2] to scan at 10°, 30°, and 50° at 15 GHz. Good agreement is observed between the scanning predicted from the TEN and measured results.

## References

[1] A. A. Oliner and D. R. Jackson, , J. L. Volakis, Ed., "Leaky-wave antennas," in *Antenna Engineering Handbook*, 4th ed. New York, NY, USA: McGraw-Hill, Jun. 2007, ch. 11.

[2] A. J. Martinez-Ros, J. L. Gomez-Tornero, and G. Goussetis, "Planar leaky-wave antenna with flexible control of the complex propagation constant," *IEEE Trans. Antennas Propag.*, vol. 60, no. 3, pp. 1625–1630, Mar. 2012.

[3] A. A. Oliner, "Leakage from higher modes on microstrip line with application to antennas," *Radio Sci.*, vol. 22, pp. 907–912, Nov. 1987.

[4] G. Zelinski, G. Thiele, M. Hastriter, M. Havrilla, and A. Terzuoli, "Half width leaky wave antennas," *Microw. Antennas Propag.*, vol. 1, no. 2, pp. 341–348, Apr. 2007.

[5] E. Kuester, R. Johnk, and D. Chang, "The thin-substrate approximation for reflection from the end of a slab-loaded parallel-plate waveguide with application to microstrip patch antennas," *IEEE Trans. Antennas Propag.*, vol. AP-30, no. 5, pp. 910–917, Sep. 1982.

[6] N. Marcuvitz, *Waveguide Handbook*. Stevenage, U.K.: Peregrinus, 1986.

[7] F. Xu and K. Wu, "Guided-wave and leakage characteristics of substrate integrated waveguide," *IEEE Trans. Microw. Theory Tech.*, vol. 53, no. 1, pp. 66–73, Jan. 2005.

[8] F. D. Quesada Pereira, V. E. Boria Esbert, J. Pascual García, A. Vidal Pantaleoni, A. Álvarez Melcón, J. Gómez Tornero, and B. Gimeno Martínez, "Efficient analysis of arbitrarily shaped inductiveobstacles in rectangular waveguides using a surface integral equation formulation," *IEEE Trans. Microw. Theory Tech.*, vol. 55, no. 4, pp. 715–721, Apr. 2007.

[9] H. Shigesawa, M. Tsuji, P. Lampariello, F. Frezza, and A. Oliner, "Coupling between different leaky-mode types in stub-loaded leaky waveguides," *IEEE Trans. Microw. Theory Tech.*, vol. 42, no. 8, pp. 1548–1560, Aug. 1994.

[10] J. Gomez-Tornero, A. delaTorreMartinez, D. Rebenaque, M. Gugliemi, and A. Alvarez-Melcon, "Design of tapered leaky-wave antennas in hybrid waveguide-planar technology for millimeter waveband applications," *IEEE Trans. Antennas Propag.*, vol. 53, no. 8, pp. 2563–2577, Aug. 2005.